COMMUNICATIONS IN COMPUTATIONAL PHYSICS
Vol. **2**, No. 2, pp. 255-270

Commun. Comput. Phys.
April 2007

The Construction of Simulation Algorithms for Laser Fusion

Wenbing Pei*

Institute of Applied Physics and Computational Mathematics, P. O. Box 8009, Beijing 100088, P. R. China.

Received 7 November 2005; Accepted (in revised version) 20 May 2006

Available online 30 September 2006

Abstract. In this work, we will present a system of numerical simulations for inertial confinement fusion, which consists of a series of one-dimensional, two-dimensional and three-dimensional codes. Our efforts have been made to develop 2D and 3D computer simulation codes, forming a 2D simulation capability so with the key physics issues in laser fusion can be separately simulated mainly by a LARED family containing six different 2D (and partially 3D) code series. The models and the characteristics of the main codes will be described, and some simulation results using the LARED family will be presented.

PACS: 41.75.Jv, 52.38.-r, 02.70.-c

Key words: Laser fusion, numerical simulations, LARED.

1 Introduction

Laser fusion, belonging to inertial confinement fusion (ICF), uses a high power laser as a driver to implode capsules filled with fusion fuel and produce thermonuclear energy. The capsule implosion is driven by either electron ablation (direct drive) or radiation ablation (indirect drive). In the direct drive, the laser beams are aimed directly at the capsule. In the indirect drive, the laser energy is first absorbed in a high-Z enclosure, a hohlraum. The hohlraum wall converts most of the laser energy into x rays which ablate the capsule at the hohlraum center and drive implosion.

Substantial progress has been made in the past and it is likely that the ignition condition will be achieved in the laboratory within the next decade. The target design of ignition used in both the National Ignition Facility (NIF) in the US [1] and the Laser

*Corresponding author. *Email address:* pei_wenbing@iapcm.ac.cn (W. Pei)

Table 1: Description of the LARED code family.

Names	**Function**
LARED–P	2D and 3D PIC parallelized code for laser plasma interaction.
LARED–H	2D non-LTE radiation hydrodynamic ALE code for Laser-target coupling and hohlraum physics.
LARED–R	2D code for radiation transport
LARED–I	2D code for indirect driven approach implosion dynamics, ignition and burn propagation.
LARED–D	2D code for direct and indirect driven approach implosion dynamics, ignition and burn propagation.
LARED–S	2D and 3D Eulerian code series for hydrodynamic instability.

Mega Joule (LMJ) in France [2] is preferable to the indirect drive approach because the x-ray drive is of high uniformity and easy to be used for other applied and basic researches such as in high energy density physics.

Physics of laser fusion involves very complicated physical processes, in particular for the indirect drive approach including the hohlraum physics and capsule physics. The hohlraum physics includes laser propagation and absorption, laser-plasma nonlinear interaction, non-local electron heat conduction, hohlraum plasma dynamics, non-LTE atomic physics, x-ray conversion and radiation transport, and hohlraum radiation field uniformity. The capsule physics includes radiation ablation, drive symmetry and hydrodynamic instability, and ignition physics. These processes with different characteristic length scales and time scales are coupled and compete with each other. Laser fusion is therefore a complicated multi-material, multi-physics (more than one physical process) and high non-LTE issue. It has been realized that computer simulations are useful in better understanding laser fusion physics, in helping the design of experiments and in analyzing the complicated results.

A system of numerical simulation for ICF research has been set up in our institute, which consists of a series of one-dimensional (1D), two-dimensional (2D) and three-dimensional (3D) codes. The 1D code series is relatively all-round in physical modeling and has been used successfully in a variety of applications. In the last decade, much effort has been made to develop 2D and 3D computer simulation codes, forming 2D simulation capability so that the key physics issues on laser fusion can be separately simulated mainly by a LARED code family containing six different 2D (and partially 3D) code series. Our simulation capability for the indirect drive laser fusion and some other applications are illustrated in Fig. 1; while some useful descriptions of the LARED codes are summarized in Table 1. In the LARED codes, LARED-H is a two-dimensional non-LTE radiation hydrodynamic code for laser-target coupling and hohlraum physics modeling. Using the hohlraum radiation drive provided by the LARED-H calculation, we can perform simulations on capsule implosion and other application problems such as hydrodynamic instability, radiation flux, opacity, equation of state (EOS), and so on. The capsule implosion process is simulated by both LARED-I and LARED-D which are two-dimensional radi-

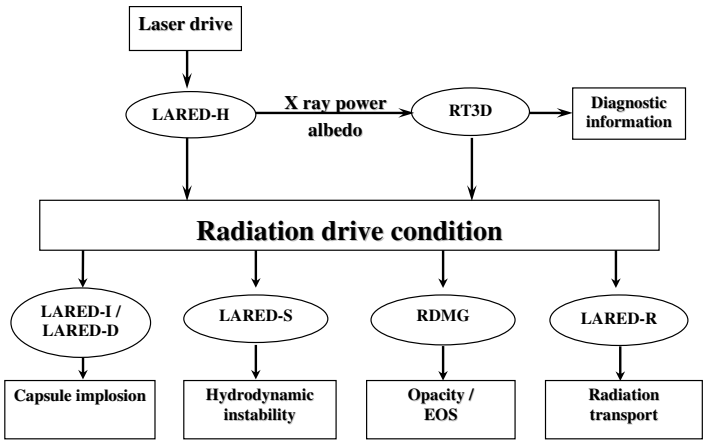

Figure 1: The illustration of numerical simulation capability for the indirect drive laser fusion and other application.

ation hydrodynamic codes in cylindrical and spherical coordinate systems, respectively. It is noted that the LARED-D is often used for the direct driven approach. The LARED-R is a two-dimensional multi-group radiation hydrodynamic code, while LARED-S, a 2D and 3D parallelized Eulerian radiation hydrodynamic code series, is designed to study hydrodynamic instability in plane, cylinder and sphere geometry. Besides the LARED, two more codes are often used in our simulation and are also listed in Fig. 1. One is RDMG [3], an 1D radiation hydrodynamic code with the radiation treated by models of transport, diffusion and conduction, which is used for solving problems such as laser-target coupling physics, capsule physics, radiation transport, radiation ablation, shock, and so on. Another is RT3D, an 3D code based on radiation transport without fluid motion, which gives an 3D irradiation asymmetry around capsule.

The LARED-P, a 2D and 3D parallelized particle-in-cell (PIC) code series, is developed to study laser-plasma interaction (LPI). The LPI impacts a wide range of physics issues, including hohlraum energetics, implosion symmetry and pulse shaping in a variety of ways. Since laser-plasma interaction problems have different time and length scales from those of radiation hydrodynamics behavior, it is difficult to be incorporated in the integrated radiation hydrodynamic simulations. The LPI effect is estimated with a PIC code or a fluid code under the plasma condition provided by the integrated simulation. An 3D fluid code is in progress because the PIC code is difficult in simulating LPI in a large length scale plasma. The LARED-P is also used to study the generation and propagation of a relativistic electron beam [4-6] which are key issues for laser fusion fast ignition. More results on LARED-P will be published elsewhere.

The rest of the paper is organized as follows. In Section 2, some details of the LARED codes, except the LARED-P and the RT3D, will be described. A number of typical simulation examples using the LARED codes will be reported in Section 3. Some concluding remarks will be given in the final section.

2 Radiation hydrodynamics codes

In laser fusion, high temperature plasma behavior is closely related to the energy transport processes due to charge particles and radiations, so the radiation hydrodynamics is the common basis of all of the LARED codes except the LARED-P which is developed by our group. The main difference between the hydrodynamic codes of LARED is about description of radiation and atomic processes and numerical methods used. In this section, we take LARED-H as an example to describe the physics models and the methods used to solve the equations, and we present the differences between the LARED-H and the other codes.

2.1 LARED-H

The LARED-H is used to study laser target coupling and hohlraum physics. It assumes that the electrons, ions and radiation field are respectively in LTE, each having its own temperature, called three-temperature approximation. The three-temperature hydrodynamic equations are

$$\frac{\partial \rho}{\partial t}+\nabla\cdot(\rho\mathbf{u})=0, \tag{2.1}$$

$$\frac{d\mathbf{u}}{dt}+\nabla(P_e+P_i+P_r)=0, \tag{2.2}$$

$$C_{ve}\frac{dT_e}{dt}+T_e\left(\frac{\partial P_e}{\partial T_e}\right)_\rho\frac{d}{dt}\left(\frac{1}{\rho}\right)=-\frac{1}{\rho}\nabla\cdot\mathbf{F_e}+W_L-W_{er}-W_{ei}, \tag{2.3}$$

$$C_{vi}\frac{dT_i}{dt}+T_i\left(\frac{\partial P_i}{\partial T_i}\right)_\rho\frac{d}{dt}\left(\frac{1}{\rho}\right)=-\frac{1}{\rho}\nabla\cdot\mathbf{F_i}+W_{ei}, \tag{2.4}$$

$$C_{vr}\frac{dT_r}{dt}+T_r\left(\frac{\partial P_r}{\partial T_r}\right)_\rho\frac{d}{dt}\left(\frac{1}{\rho}\right)=-\frac{1}{\rho}\nabla\cdot\mathbf{F_r}+W_{er}, \tag{2.5}$$

where

$$\frac{d}{dt}\equiv\frac{\partial}{\partial t}+\mathbf{u}\cdot\nabla,$$

d/dt and $\partial/\partial t$ are the time derivatives in the Lagrangian and Eulerian frames, respectively. In (2.1)-(2.5), ρ is the mass density, $\mathbf{u}$ the flow velocity, (P_e,T_e,C_{ve}), (P_i,T_i,C_{vi}), and (P_r,T_r,C_{vr}) are pressure, temperature and specific heats for the electron, ion and radiation, respectively; $\mathbf{F}_e$, $\mathbf{F}_i$, and $\mathbf{F}_r$ are heat fluxes with the flux-limited approximation for the electron, ion and radiation, respectively. Moreover, W_L is the laser energy term, which is given with a 3D ray-tracing package for computing the inverse-bremsstrahlung energy deposition rate. Besides a laser source, many possible sources can be applied either in the energy equations or in boundary conditions on temperature, flux, pressure, etc. W_{ei} is the electron-ion energy exchange term, and W_{er} is the electron-radiation energy

exchange term defined by

$$W_{er}=\frac{4\pi}{\rho}\int\left[j_\nu(T_e)\left(1+\frac{c^2}{2h\nu^3}I_{\nu p}(T_r)\right)-\mu_\nu(T_e)I_{\nu p}(T_r)\right]d\nu, \tag{2.6}$$

where $I_{\nu p}(T_r)$ is the Planck distribution $j_\nu(T_e)$ and $\mu_\nu(T_e)$ are the emission rate and absorption coefficient, respectively, which consist of contributions from free-free, bound-free, and bound-bound transitions of electrons. $j_\nu(T_e)$ and $\mu_\nu(T_e)$ are determined after specifying the atomic state of the plasmas by using the screened hydrogenic average-atom model. The thermodynamic quantities are derived either from the ideal gas model or from data of realistic equation of state.

The code LARED-H can model a 2D axial symmetry system or a 2D Cartesian system by introducing a relation $R=1-\alpha+\alpha y$ by defining the operators

$$\nabla f=\frac{\partial f}{\partial x}\vec{i}+\frac{\partial f}{\partial y}\vec{j},\quad \nabla\cdot\vec{F}=\frac{\partial F_x}{\partial x}+\frac{1}{R}\frac{\partial RF_y}{\partial y},\quad dV=Rdxdy, \tag{2.7}$$

where $\alpha=0$ (i.e., $R=1$) corresponds to the 2D Cartesian system; $\alpha=1$ (i.e., $R=y$) corresponds to the 2D axial symmetry system. The LARED-H is designed on a structured mesh on multi-regions with different resolution requirements. The Arbitrary Lagrangian Eulerian (ALE) method [7] with staggered grid is used. The discrete time rezoning is also provided and allows an arbitrary overlap between the old and new mesh. The electron, ion and radiation thermal conduction equations are solved on the arbitrary quadrilateral mesh with Kershaw's nine-point diffusion difference scheme [8].

2.2 LARED-I

The LARED-I is a 2D axially symmetric three-temperature Lagrangian hydrodynamic code for studying indirect drive implosion physics. The radiation sources are imposed in the radiation equation or in the boundary conditions on temperature or flux. The atomic processes are assumed to be in LTE and the average ionization degree and W_{er} are calculated with the Fermi-Dirac distribution, or obtained from the data tables. Ignition and burn dynamics are considered. Neutrons are assumed to escape from system as soon as they are generated. The hydrodynamic equations are solved with the supporting operator method [9].

2.3 LARED-D

The LARED-D models direct and indirect drive implosion described in a 2D spheric coordinate system. The basic equations are the three-temperature hydrodynamic equations. The laser energy deposition is calculated in geometry optics approximation along the radial direction. The hydro equations are solved with both the implicit and explicit difference schemes.

2.4 LARED-R

The LARED-R is an 2D radiation transport and diffusion Lagrangian hydrodynamic code in axially symmetric cylinder coordinate. Its main difference from LARED-H is that the radiation field is not assumed to be Planckian and is described by the frequency-dependent transport and/or diffusion equations,

$$\begin{aligned}&\frac{1}{c}\frac{\partial I_\nu}{\partial t}+\mathbf{\Omega}\cdot\nabla I_\nu=\mu'_\nu(T_e)[I_{\nu p}(T_e)-I_\nu],\\&\frac{1}{c}\frac{\partial I_\nu}{\partial t}+\nabla\cdot\frac{1}{3\mu'_\nu(T_e)}\nabla I_\nu=\mu'_\nu(T_e)[I_{\nu p}(T_e)-I_\nu].\end{aligned}\tag{2.8}$$

Users can choose multigroup transport, multigroup diffusion, or thermal conduction for the radiation field in different regions, according to the needs of the physical problem studied. The plasma is assumed to be in LTE and the average ionization degree and the radiation parameters are calculated with the Fermi-Dirac distribution, or obtained from the data tables. The radiation transport equation is solved with the discrete ordinate method [10].

2.5 LARED-S

The LARED-S is a multi-dimensional (2D and 3D in planar, cylindrical and spherical geometries), multi-material, Eulerian radiation hydrodynamic code series with movable mesh. The users can choose multigroup diffusion or thermal conduction to model radiation. The operator splitting method is used to treat each of the physical processes.

The basic hydrodynamic algorithm is the flux-corrected transport method (FCT) [11, 12] with sixth-order phase errors on a locally uniform grid, capturing shocks with corrected antidiffusive flux, or the piecewise-parabolic method (PPM) [13] with third-order accuracy. The implementation of PPM in this code is in two steps, namely a Lagrangian hydrodynamic step coupled with a re-mapping step (from the Lagrangian grid to the Eulerian grid). Two different mixing physical models are used for multi-material problems, one is the volume of fluid (VOF) interface reconstruction method [14] based on the PPM scheme, and the other is the consistent multi-fluid advection (CMA) method [15] based on the FCT or PPM scheme.

2.6 RT3D

The RT3D, an 3D radiation transport code [16], is developed to study hohlraum radiation drive symmetry around capsule and other sample packages. In the RT3D, the hydrodynamic equations are not solved and the plasma condition in the hohlraum is given in advance. Assume the hohlraum wall (including the capsule if there is one) to be optically thick. The wall is described by using the power balance relationship

$$F_{in}+S_{in}=F_{out}+\dot{E}_{wall},\tag{2.9}$$

where F_{in} and F_{out} denote the radiation fluxes into and out of the wall cell, respectively, S_{in} is the radiation source flux converted from the laser beams which is known, E_{wall} is the energy absorbed by the wall which is associated with the wall cell temperature by scaling relation, $E_{wall}=\alpha T^{\beta}t^{\gamma}$.

The radiation field is described by the transport equation (2.8) in grey approximation. Assume the emission from wall is Lambertian, and the boundary conditions are

$$\begin{aligned} &F_{in}(\mathbf{r},t)=\sigma T^4(\mathbf{r},t)=\int_{\mathbf{n}\cdot\mathbf{\Omega}>0} I(\mathbf{r},\mathbf{\Omega},t)\mathbf{n}\cdot\mathbf{\Omega}d\Omega,\\ &I(\mathbf{r},\mathbf{\Omega},t)=\frac{1}{\pi}F_{out}(\mathbf{r},t)=\frac{1}{\pi}(F_{in}+S_{in}-\dot{E}_{wall}),\quad \text{for } \mathbf{n}\cdot\mathbf{\Omega}<0, \end{aligned} \tag{2.10}$$

where $\mathbf{n}$ is the normal of the wall element, and σ is the Stefan-Boltzmann constant. Eq. (2.8) is discretized with the implicit difference method, and the corresponding geometry factors, which are the transport probabilities of particles from one element to another one, are calculated using the Monte Carlo method.

3 Typical simulation examples

3.1 Simulations of laser target coupling and hohlraum physics

Some LARED-H simulation results are shown in this section. Since either the cylindrical coordinate or the Cartesian coordinate is used, the LARED-H can simulate the problems of both hohlraum and disk irradiated by an obliquely incident laser. In the following example, the Au disk is irradiated by a 0.35μm Gaussian laser pulse of intensity of 1.5×10^{14} Wcm^{-2} and FWHM of 0.6ns. The laser incident angle is 45°, and the peak time is 0.8ns. Fig. 2 shows the meshes at the end of the laser pulse ($t=$1.4ns), which indicates that the plasma mainly blows off along the normal of the disk despite existing lateral rarefaction.

We use LARED-H to simulate the hohlraum experiments on Shenguang II (SG-II) [17,18]. Eight beams, four per side, enter the gold hohlraum through laser entrance holes (LEHs) at the ends of the cylinder at angle of 45° to the symmetry axis. The SG-II standard hohlraums are 1400μm long and 800μm diameter with 380μm diameter LHEs. The hohlraums are heated with 0.35μm laser in a 1.0ns square pulse with 2.0-2.5kJ of laser energy. The radiation temperature is measured by Dante at 30° to the hohlraum axis outside the LEH. Fig. 3 shows the mesh of SG II hohlraum at $t=$1.0ns. Four snapshots of electron density, electron temperature, laser energy deposition and x-ray conversion at $t=1.0$ns are shown in Fig. 4. The plasma mainly moves along the radius direction and it is faster if it originates from the laser spots (around z=400μm). The electron density in the hohlraum is uniform and equal to around $0.1n_c$ ($n_c=9\times10^{21}$cm^{-3}) except for the stagnation region where the electron density is a little higher (see Fig. 4(a)). The laser energy deposition (Fig. 4(c)) and x-ray conversion (Fig. 4(d)) dominate in the neighborhood

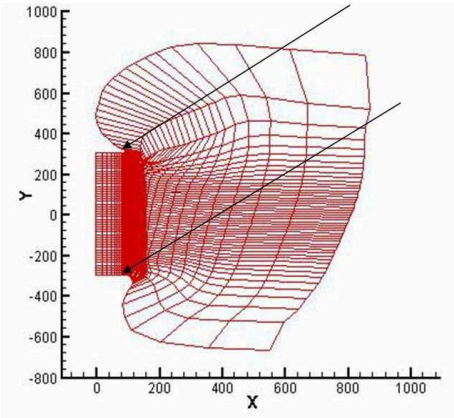

Figure 2: The mesh of disk with incident angle of 45° at the end of laser pulse (t=1.4ns).

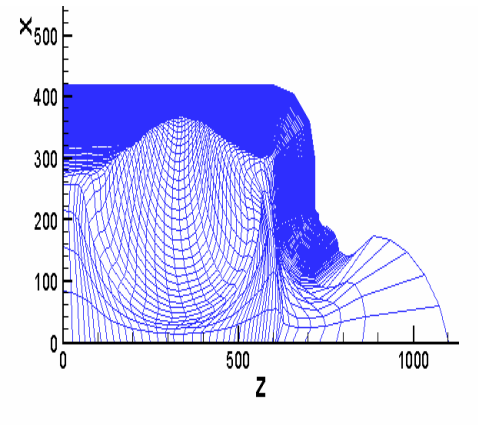

Figure 3: The mesh of SG II hohlraum at t=1.0ns.

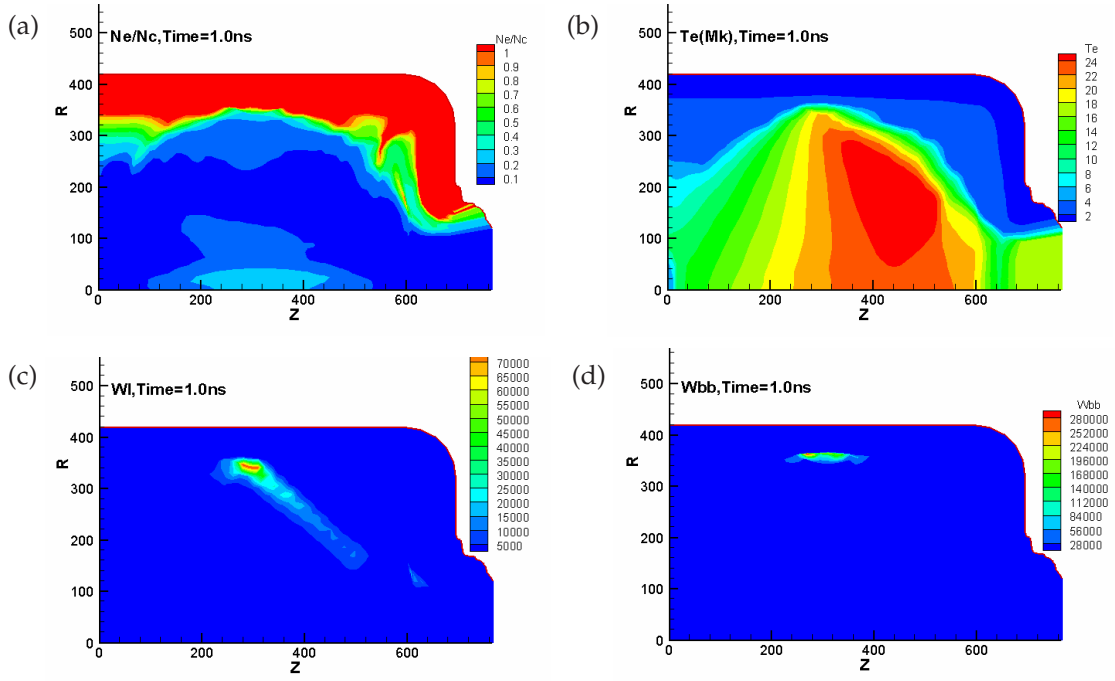

Figure 4: The snapshots of (a) electron density, (b) electron temperature, (c) laser energy deposition and (d) x-ray conversion, at t=1.0ns.

of the critical surface (where $n_e = n_c$) near the initial wall position. The LARED-H calculations are postprocessed to mimic the Dante view to give the radiation temperature as shown in Fig. 5. The agreement between the measured and calculated drive temperature of the SG II is very good around the peak.

The hohlraum drive uniformity around the capsule or the sample package can be

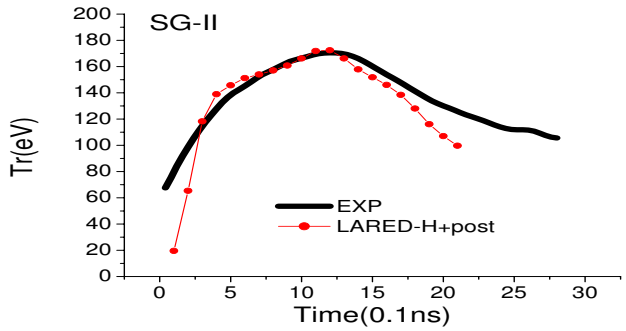

Figure 5: Measured and simulated Dante drive temperature of the SG II experiment versus time.

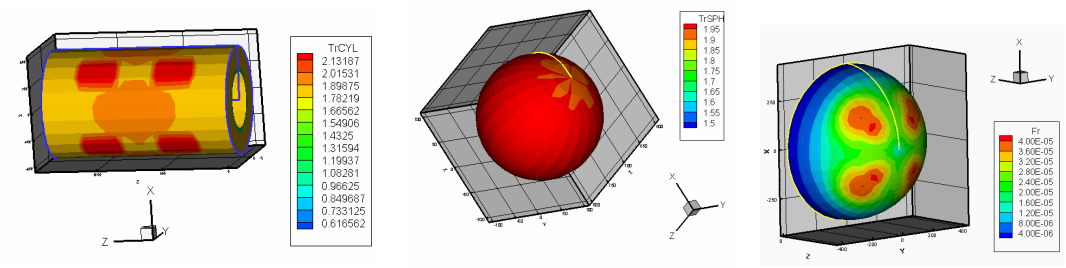

(a) (b) (c)

Figure 6: The RT3D simulation of SG II hohlraum with capsule: the radiation temperature (in 10^6K) distribution on the internal wall (a) and on the capsule (b), and the flux onto the chamber from the LEH (c).

simulated with RT3D. Fig. 6 shows the RT3D simulation of SG II hohlraum with capsule. The RT3D can provide not only the radiation temperature distribution on the inner wall (Fig. 6(a)) and on the capsule (Fig. 6(b)), but also the flux from the LEH or the diagnostic hole received by detectors on the chamber (e.g., Fig. 6(c)). The nonuniformity of temperature on the capsule is about 2% although the hot spots on the wall are hotter.

3.2 Simulations of capsule implosion

Indirect drive implosion

The radiation drive implosion process is simulated with the LARED-I according to the drive condition provided by the RT3D. Fig. 7 shows the LARED-I calculations of modeling symmetry for Nova experiments [19]. For these experiments, the beam crossing position is fixed in the plane of the LEH, so the drive symmetry on the capsule changes with the hohlraum length due to the fixed laser incident angle. The capsule distortion, characterized by the ratio of the capsule waist dimension to the dimension along the hohlraum axis, is plotted versus the hohlraum half-length. As observed in Fig. 7, the LARED-I calculations are in good agreement with the results of the Nova experiments and the LASNEX calculations.

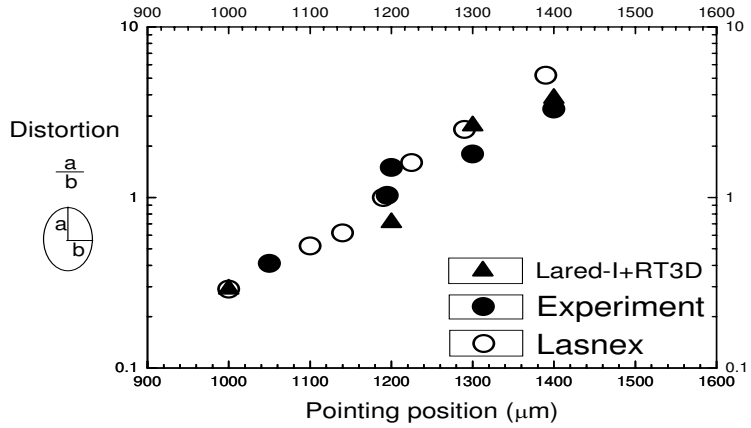

Figure 7: The simulation results of LARED-I are in good agreement with the results of Nova experiments and LASNEX calculations.

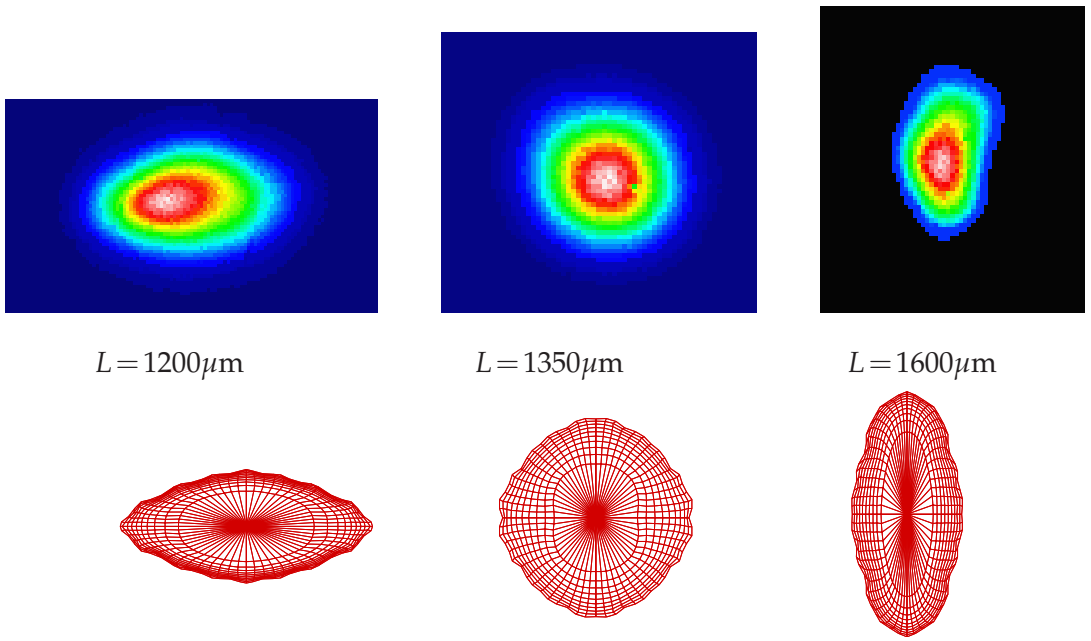

Figure 8: Comparison between SG II experiments (top) and the LARED-I calculations (bottom).

Fig. 8 shows the results of the SG II experiments and the LARED-I calculation. For these experiments, SG II standard hohlraums with $300\times300\mu$m^2 diagnostic hole are used, and the plastic capsules are 150μm radius and 12-15μm thick with doped Ar in D_2 fill. The hohlraum length changes from 1200μm to 1600μm. The capsule distortion recorded by frame x-ray camera from the diagnostic hole is shown in the top row of Fig. 8, and the LARED-I results in the bottom row. The agreement in shape between the experimental results and the LARED-I calculations is good.

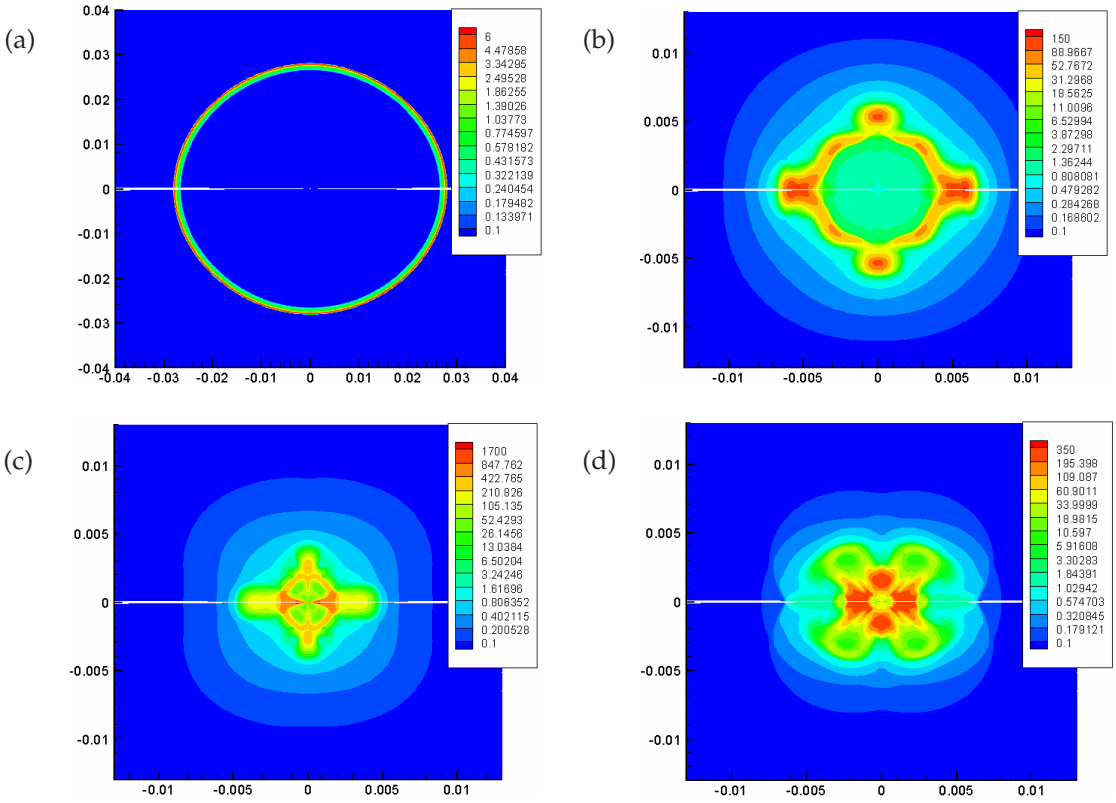

Figure 9: Density profiles of the asymmetric laser-driven implosion at different phase with the LARED-S calculations: (a) prepulse, (b) acceleration phase, (c) deceleration phase, and (d) rebound phase.

Direct drive implosion

The capsule implosion is simulated with the LARED-S code. Fig. 9 shows the result of asymmetric laser-driven implosion. The capsule has an outer radius of 325 microns. The polystyrene ablator is 25 microns thick at a density of $1g/cm^3$, and the capsule center is filled with the D_2 gas at a density of $1mg/cm^3$. The pulse delivers about 10kJ of laser light at the SG-II upgrading set. The laser intensity has a perturbation with 5% fluctuation in the polar angle direction.

The fast ignition implosion is simulated with the LARED-S code. The capsule has an outer radius of 325 microns. The polystyrene ablator is 25 microns thick at a density of $1g/cm^3$, and the capsule center is filled with the D_2 gas at a density of $1mg/cm^3$. The reentrant copper cone has an opening angle 60° and the tip 50 microns from the center of the capsule. The capsule is driven with the 10kJ of laser light at the SG II upgrading set. Fig. 10 shows the density and temperature profiles without and with perturbation on the target surface.

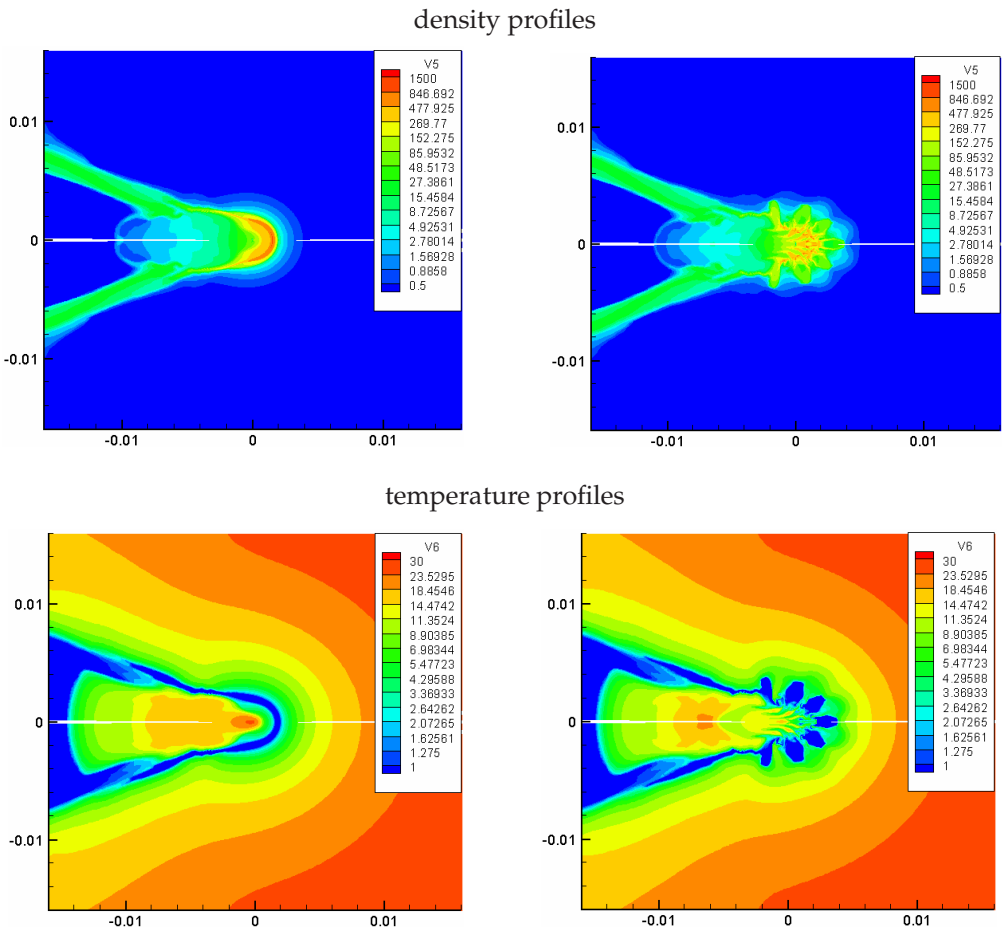

Figure 10: Density and temperature profiles of the fast ignition implosion with the LARED-S calculations, left: without perturbation, and right: with perturbation.

3.3 Simulations of Hydrodynamic instability

The LARED-S can also be used to simulate the hydrodynamic instabilities. In Fig. 11, the result of the Richtmyer-Meshkov (R-M) instability using the LARED-S code is compared with those obtained using the ASCI codes including RAGE, Front-Tracking and FLASH. The two materials are beryllium on the right, with an initial density of 2.4g/cm^3, and foam on the left, with an initial density of 0.12g/cm^3. The initial amplitude of the perturbation is 25 microns, which is one tenth of the wavelength. A Mach 15 shock propagating from right to left is used to accelerate the interface. The LARED-S calculation agrees well with those of the ASCI codes in the physical characteristic quantities.

The shock-bubble interaction simulations of the LARED-S are compared with experiments performed by Nuclear Research Center in Israel [21], see Fig. 12. The Helium bubble in the air is used for light bubble interaction. The shock wave strength is 1.22Mach.

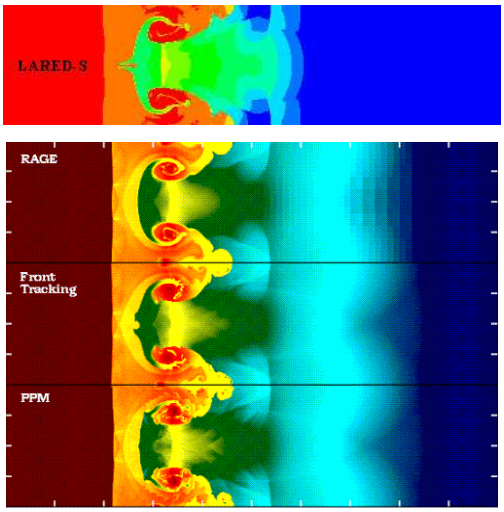

Figure 11: Richtmyer-Meshkov stability: comparison of the LARED-S calculation with those of the ASCI codes (RAGE, Frontier and FLASH).

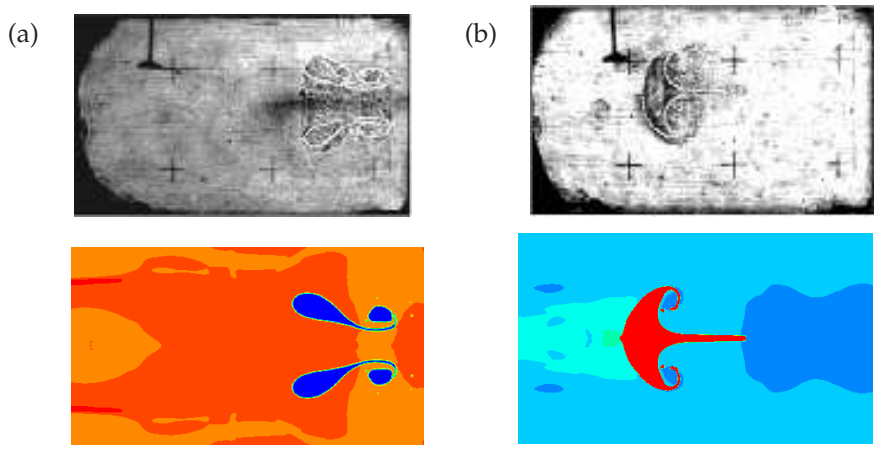

Figure 12: Comparison between shock-tube experiments and the LARED-S calculations: (a) light bubble, (b) heavy bubble.

SF_6 bubble in the air is used for heavy bubble interaction. The shock wave strength is 1.17Mach. Comparison shows that the LARED-S calculation results are in good agreement with the shock-bubble experiment results.

3.4 Simulations of supersonic radiation transport

Radiation transport is a very important process in both ICF and astrophysics, which is rather complicated due to the strong coupling of radiation with matter. In order to un-

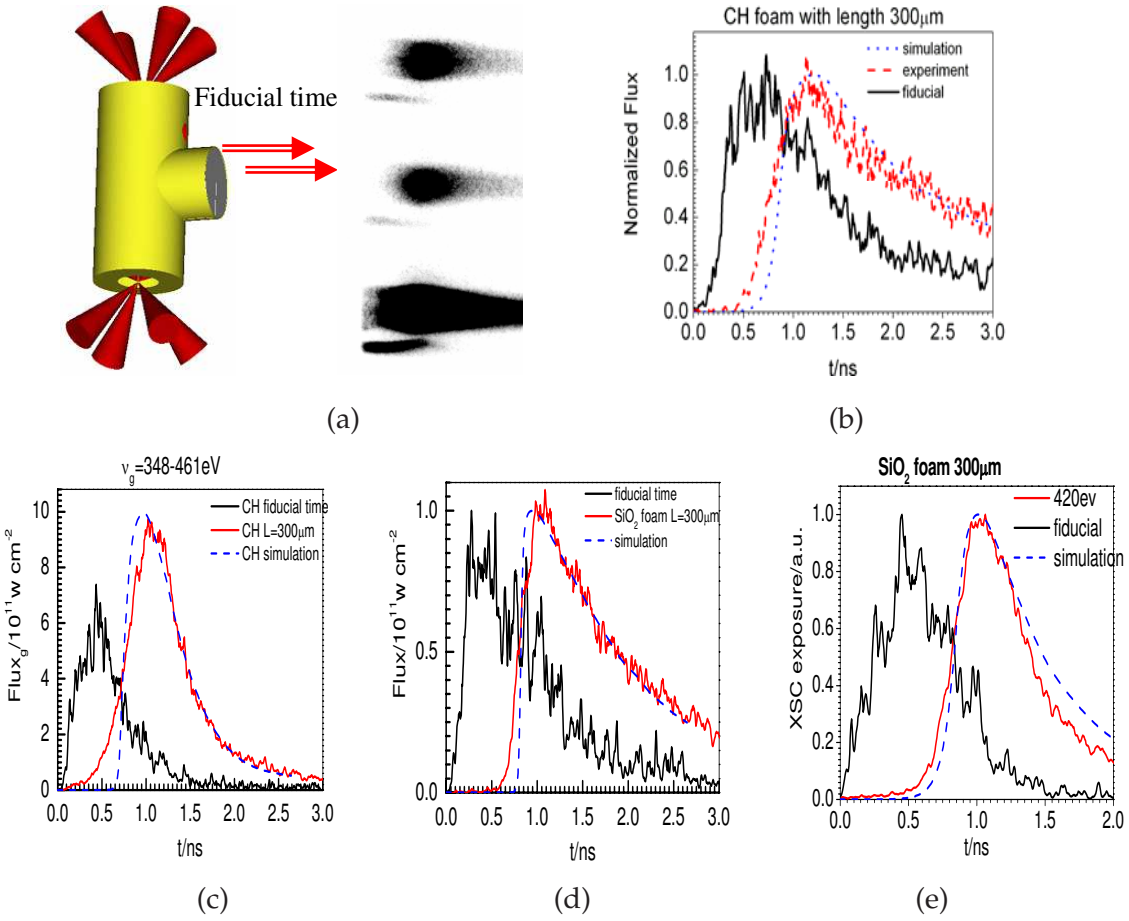

Figure 13: The comparison between the LARED-R-1 simulation results and the experiment of supersonic radiation transfer in low-density foam done on the SG II laser facility. The density of foam is 0.05g/cm^3.(a): Experiment setting; (b): the transfer of 210eV group in CH foam 300μm, (c): the transfer of 420eV group in CH foam 300μm, (d): the transfer of 210eV group in SiO_2 foam 300μm, and (e): the transfer of 420eV group in SiO_2 foam 300μm.

derstand the radiation transport mechanism and validate the codes, the experiments [22] of radiation supersonic propagation in low-density foam filled in high Z tube have been carried out in SG-II laser facility. The experiment setting is shown in Fig. 13. The tube is 300μm long and filled with 0.05g/cm^3 CH or SiO_2 foam. The radiation propagation time at 210eV and 420eV is measured. The comparison between the results of experiment and the LARED-R simulation is given in Fig. 13, which is found in good agreement.

The LARED-R is also used to simulate the experiments of supersonic radiation flow performed on the OMEGA laser facility by Back et al. [23]. The simulation result is in good agreement with the experimental result and the LASNEX calculation, see [24].

4 Summary

In the last decade, we have developed a series of 2D and 3D computer simulation codes for laser fusion. In this paper, some of the typical simulation results are presented. The LARED-H calculations of the SG-II hohlraum show that the results about plasma state, laser absorption and the x-ray conversion are acceptable and that the calculated radiation temperature is in good agreement with the measured one. Under the radiation drive conditions provided by RT3D, the LARED-I calculations for the capsule distortion are found comparable with the experimental results. Moreover, the LARED-S has been demonstrated useful in simulating capsule implosion and hydrodynamic instability. In particular, it has been used successfully in simulating the Richtmyer-Meshkov instability and the shock-bubble interaction simulations. The LARED-R can reproduce the experimental results for radiation propagation in a tube filled with low density.

In conclusion, we have built a 2D simulation capability useful in simulating some of the key physics issues in the research of laser fusion such as laser plasma interaction, hohlraum physics, drive symmetry, capsule implosion physics and so on. It is based on the LARED family containing six different 2D (and partially 3D) code series and the 3D radiation transport code RT3D. The comparisons between the simulation and experiment results indicate that our codes are reliable.

We are now in the process of developing the integrated 2D simulation capability for laser fusion with a variety of optional physics models and numerical methods.

Acknowledgments

I would like to acknowledge the contributions of my colleagues who contributed to the development of the codes described in this paper. This work was supported by the National Hi-Tech Inertial Confinement Fusion Committee of China, by the National Natural Science Foundation of China under Grant No. 10335020, and by the National Basic Research Program under the Grant 2005CB321702.

References

[1] J. A. Paisner, E. M. Campbell and W. J. Hogan, The national ignition facility protect, Fusion Technol., 26 (1994), 755.
[2] P. A. Holstein, F. Chaland, C. Charpin, J. M. Dufour, H. Dumont, J. Giorla, L. Hallo, S. Laffite, G. Malinie, Y. Saillard, G. Schurtz, M. Vandenboomgaerde and F. Wagon, Evolution of the target design for the MJ laser, Laser Part. Beams, 17 (1999), 403.
[3] P. Gu, W. Pei, T. Feng and C. Wu, Investigation on non-LTE radiation emitted from a laser-irradiated Au disk, Sci. China Ser. G, 48 (2005), 345.
[4] C. Y. Zheng, S. P. Zhu and X. He, Quasistic magnetic field generation by intense ultrashort laser pulse in underdense plasma, China Phys. Lett., 17 (2000), 746.

[5] C. Y. Zheng, X. T. He and S. P Zhu, Magnetic field generation and relativistic electron dynamics in circularly polarized intense laser with dense plasmas, Phys. Plasmas, 12 (2005), 044505.
[6] C. Y. Zheng, Z. J. Liu, S. P. Zhu, A. Q. Zhang and X. T. He, Simulation of electron beam instabilities in collisionless plasmas, J. Plasma Phys., 72(2) (2006), 249.
[7] C. W. Hirt, A. Amsden and J. Cook, An arbitrary Larangian-Eulerian computing method for all flow speeds, J. Comput. Phys., 14 (1974), 227.
[8] D. S. Kershaw, Differencing of the diffusion equation in Lagrangian hydrodynamic codes, J. Comput. Phys., 39 (1981), 375.
[9] E. J. Caramana, D. E. Burton, M. J. Shashkov and P. P. Whalen, The construction of compatible hydrodynamics algorithms utilizing conservation of total energy, J. Comput. Phys., 146 (1998), 227.
[10] S. Chandrasekhar, Radiative Transfer, Dover, New York, 1960.
[11] J. P. Boris and D. L. Book, Flux-corrected transport I: SHASTA, a fluid transport algorithm that works, J. Comput. Phys., 11 (1973), 38.
[12] J. F. Wu, W. H. Ye and W. Y. Zhang, Numerical study of Rayleigh-Taylor instability, High Power Laser Part. Beams, 15 (2003), 64, in Chinese.
[13] P. Collela and P. R. Woodward, The piecewise parabolic method (PPM) for gas-dynamical simulations, J. Comput. Phys., 54 (1984), 174.
[14] D. L. Youngs, Time dependent multi-material flow with large fluid distortion, in: K. W. Morton and M. J. Baines (Eds.), Numerical Methods for Fluid Dynamics, Academic Press, New York, 1982, pp. 273-285.
[15] T. Plewa and E. Muller, The consistent multi-fluid advection method, Astron. Astrophys., 342 (1999), p. 179.
[16] T. Feng, and D. Lai, Sci. China Ser. E, 26 (1996), 376.
[17] T. Chang, Y. Ding, D. Lai, T. Huan, S. Zhu, Z. Zheng, G. Wang, Y. Zheng, X. He, W. Pei, Q. Duan, W. Zhang, T. Feng, G. Chen and P. Gu, Laser hohlraum coupling efficiency on the Shenguang II facility, Phys. Plasmas, 9 (2002), 4744.
[18] T. Chang, G. Wang, Y. Li, J. Sheng and W. Pei, Inferring the capsule-absorbed radiation energy from experimental hohlraum radiation temperature, Phys. Plasmas, 11 (2004), 4286.
[19] J. Lindl, Development of the indirect-drive approach to inertial confinement fusion and the target physics basis for ignition and gain, Phys. Plasmas, 2 (1995), 3933.
[20] R. L. Holmes, G. Dimonte, B. Fryxell, M. L. Gittings, J. W. Grove, M. Schneider, D. H. Sharp, A. L. Velikovich, R. P. Weaver and Q. Zhang, Richtmyer-Meshkov instability growth: Experiment, simulation and theory, J. Fluid Mech., 389 (1999), 55.
[21] K. Levy, O. Sadot, A. Rikanati, D. Kartoon, Y. Srebro, A. Yosef-Hai, G. Ben-Dor and D. Shvarts, Scaling in the shock-bubble interaction, Laser Part. Beams, 21 (2003), 335.
[22] Y. Xu, D. Lai, S. Li, T. Feng, K. Lan, J. Li, W. Pei and T. Chang, Theoretical research on radiation transport in the foam-filled tube, Sci. China Ser. G, 34 (2004), 525, in Chinese.
[23] C. A. Back, J. D. Bauer, O. L. Landen, R. E. Turner, B. F. Lasinski, J. H. Hammer, M. D. Rosen, L. J. Suter and W. H. Hsing, Detailed measurements of a diffusive supersonic wave in a radiatively heated foam, Phys. Rev. Lett., 84 (2000), 274.
[24] K. Lan, T. Feng, D. Lai, Y. Xu and X. Meng, Study on two-dimensional transfer of radiative heating wave, Laser Part. Beams, 23 (2005), 275.

â€¢ Algorithm for construction of absolute phase map: The phase map construction algorithm generates a set of fringe patterns for projection and constructs an absolute phase map of the object surface from the corresponding images that have been taken. The algorithm we developed uses multiple fringe frequencies but requires fewer pro-jection patterns than conventional methods. It is dened on a generalized concept of phase shifting and hence is able to deal with fringe patterns with curved fringes and continuously varying fringe width. â€¢ Algorithm for construction of point cloud: The point cloud c...